Article

Highly sensitive wearable sensor based on a flexible multi-layer graphene film antenna

Danli Tang [a,1], Qianlong Wang [b,1], Zhe Wang [c,1], Quantao Liu [d], Bin Zhang [a], Daping He [a,c,*], Zhi Wu [a], Shichun Mu [c]

[a] Hubei Engineering Research Center of RF-Microwave Technology and Application, School of Science, Wuhan University of Technology, Wuhan 430070, China
[b] Shenzhen Institute of Advanced Graphene Application and Technology (SIAGAT), Shenzhen 518106, China
[c] State Key Laboratory of Advanced Technology for Materials Synthesis and Processing, Wuhan University of Technology, Wuhan 430070, China
[d] State Key Laboratory of Silicate Materials for Architectures, Wuhan University of Technology, Wuhan 430070, China

ARTICLE INFO

ABSTRACT

The use of advanced carbon nanomaterials for flexible antenna sensors has attracted great attention due to their outstanding electromechanical properties. However, carbon nanomaterial based composites have yet to overcome drawbacks, such as low conductivity and toughness. In this work, a flexible multi-layer graphene film (FGF) with a high conductivity of 10^6 S/m for antenna based wearable sensors is investigated. A 1.63 GHz FGF antenna sensor exhibits significantly high strain sensitivity of 9.8 for compressive bending and 9.36 for tensile bending, which is super than the copper antenna sensor (5.39 for compressive bending and 4.05 for tensile bending). Moreover, the FGF antenna sensor shows very good mechanical flexibility, reversible deformability and structure stability, and thus is well suited for applications like wearable devices and wireless strain sensing.

1. Introduction

The flexible antenna sensors, as the important component of wearable electronic devices [1], such as flexible displays [2–4], microfluidic devices [5], energy harvesting devices [6–9], have received wide attention from all over the world with the internet of things (IOT) fast growing. Generally, the existing commercial flexible antenna sensors are made of metal or semiconductor, but their sensitivity is quite limited [10–13]. Recently, along with the development of tele-surgery electronic gloves and robotic skin, the conventional flexible sensor cannot meet this increasing requirement, and the high-sensitivity sensor is imperative [14]. Meanwhile, the stretchability is also a limiting factor which restricts the development of the conventional flexible sensors. For example, the motion of human joints will create stretching or shrinking pressure as high as 55%, which far exceeds the detection limit of conventional flexible sensors [15].

In this context, advanced carbon materials such as carbon nanoparticles [16,17], carbon nanowire [18], carbon nanotube [19] and graphite [20] are emerged and shown to be promise can-

didates for innovative flexible sensors with enhanced performance. More recently, the new carbon allotrope graphene, attracts great attention in flexible communication due to its excellent electronic, mechanical and optical properties [21–24]. However, when graphene is used in commercial electronic devices, mono- or few-layered graphene films exhibit high sheet resistance and insufficient electrical conductivity, which greatly limits graphene applications in wireless sensors such as antennas and other passive components. On the other side, the multi-layer graphene film, after high temperature (usually more than 2,000 °C) treatment, it can exhibit a high in-plane oriented structure, which enable excellent planar electrical conductivity and low sheet resistant [25–29]. In 2012, Huang and Drzal [27] reported a multi-layer graphene nanoplatelet film with an electrical conductivity of 1.57×10^5 S/m by annealing the film that is filtered from graphite nanoplatelets suspension at high temperature. In 2014, Guo and co-workers [28] used a similar method of high temperature annealing to increase the electrical conductivity to 1.83×10^5 S/m. Most recently, Teng et al. [29] reported a multi-layer graphene film with an electrical conductivity 2.2×10^5 S/m based on ball-milling exfoliated graphene and high temperature annealing. It is important to point out that the flexibility of multi-layer graphene film is also feasible by the reported methods [30]. However, the conductivity of these graphene films is still much lower than that of metallic materials

* Corresponding author.
  E-mail address: hedaping@whut.edu.cn (D. He).
[1] These authors contributed equally to this work.

(10^7 S/m), further improvements are needed to meet the needs of portable antenna devices.

In this work, we demonstrate a flexible multi-layer graphene film (FGF) prepared by high temperature heat treatment and subsequent rolling process of a graphene oxide assembled film, achieving a significant high electrical conductivity ($\sim 10^6$ S/m, nearly comparable to metal) and good stretchability. Moreover, a 1.63 GHz rectangular microstrip patch antenna is fabricated by paving a tailored FGF patch on paper substrate. Given that advantageous features of the film, this FGF antenna exhibits excellent radiation performance (similar to copper antenna), which can be well maintained even after bending 100 times. Since the antenna deformation would result in a resonant frequency shift, a wireless strain sensor is achieved by exploiting this FGF antenna with good mechanical flexibility, reversible deformability and structure stability in healthcare. To the best of our knowledge, the FGF antenna sensor performance in terms of sensitivity compares favorably with various nanomaterials based resistive strain sensors reported so far.

2. Experimental

2.1. Preparation of flexible multi-layer graphene film

The graphene oxide (GO) suspension, which is purchased from Wuxi chengyi education technology Co. Ltd., is diluted to 10–20 mg/mL with ultrapure water, followed by scraped on polyethylene terephthalate (PET) film, evaporated at room temperature to acquire the GO film. The GO film is under high temperature annealing at 1300 °C for 2 h, thereafter 3000 °C for 1 h, both within Ar gas flow, then rolling compressed to obtain a FGF film.

2.2. Design for radiation patch

Based on microstrip antenna's transmission-line model, for a rectangular radiation patch with a resonant frequency f_{res}, the physical length L and width W are designed [31].

$$L = \frac{c}{2f_{res}\sqrt{\varepsilon_{reff}}} - 2\Delta L, \tag{1}$$

$$W = \frac{c\sqrt{2}}{2f_{res}\sqrt{\varepsilon_r + 1}}, \tag{2}$$

where

$$\varepsilon_{reff} = \frac{\varepsilon_r + 1}{2} + \frac{\varepsilon_r - 1}{2}\left(1 + 12\frac{h}{W}\right)^{-1/2}, \tag{3}$$

$$\Delta L = 0.412h\frac{(\varepsilon_{reff} + 0.3)\left(\frac{W}{h} + 0.264\right)}{(\varepsilon_{reff} - 0.258)\left(\frac{W}{h} + 0.8\right)}. \tag{4}$$

ε_r is the dielectric constant of the cellulose paper, ε_{reff} is effective dielectric constant because cellulose paper and FGF have different dielectric constant, c is the speed of light in free space and h is the thickness of the cellulose paper. ΔL is the extended length due to fringing fields at the edge of the patch which makes the actual radiation length larger than the physical length, but it can be neglected as $\Delta L \ll L$.

2.3. Device fabrication

The FGF antenna sensor is fabricated by sandwiching cellulose filter paper between FGF ground plane and rectangular patch.

2.4. Measurement device

The resonant frequency and reflection coefficient are collected using a Keysight N5225A Vector Network Analyzer (VNA). Radiation patterns are measured in the microwave anechoic chamber and VNA provides input signal. Two-dimensional (2D) pattern cuts are measured by Diamond Engineering Antenna Measurement System which is connected with VNA by General Purpose Interface Bus (GPIB). Each cut is obtained by rotating the antenna in 10° increments while recording the received signal with a broadband horn antenna as a standard reference antenna.

3. Results and discussion

FGF is prepared from GO suspension (inset of Fig. 1a), and the transmission electron microscope (TEM) image of a GO sheet is shown in Fig. 1a. After a series of processing steps (manufacturing details in the Supporting Information and Fig. S1 online), a flexible FGF (Fig. 1b) is obtained with a thickness of 30 µm (Fig. 1d). In the X-ray diffraction (XRD) pattern of FGF (Fig. 1c), a sharp and intense diffraction peak located at $2\theta = 26.5°$ indicates a $d_{002} = 0.34$ nm, and the diffraction peak of the (0 0 4) plane refers to the highly graphitization structure of FGF. The D band (1,335 cm^{-1}) and G band (1,585 cm^{-1}) can be found in Raman spectroscopy (inset of Fig. 1c), which refers to lattice defects and the characteristic sp^2 hybridized carbon atoms in graphene, respectively. After hundreds times of 180° folding and 150° bending (Fig. 1e), although some breakages occur in fold area, the FGFs remain integrated structure, exhibiting good flexibility. However, it is worth noting that the breakages occurring in fold area may be from preparation of samples rather than 180° folding. In addition, during 500 cycles bending test with bending speed of 2 Hz and bending degree of 0° (initial state) $\rightarrow$ 70° (bending state), relative volume resistances of the film almost maintain constant, suggesting the remarkable stability under mechanical deformation (Fig. 1f).

As one of the most widely used antennas, rectangular microstrip patch antenna is a two dimensional antenna that use patch as radiation part. It has a lot of advantages such as low profile, light weight, easy integration, flexible feeding, et al. Fig. 2a illustrates the rectangular microstrip patch antenna's schematic diagram consisted of a radiating patch, a ground plane and a single-layer cellulose paper between them.

In this work, the resonant frequency of the antenna f_{res} is set to 1.63 GHz and the paper's thickness h is 0.04 mm. The dielectric constant of the cellulose paper with binder $\varepsilon_r = 3.06$ is obtained based on coaxial transmission line method. So, by using the transmission-line model and then optimization, the dimensions of the FGF antenna can be obtained as 35 mm × 27.4 mm (Experimental Section). In order to match the input impedance of 50 Ω transmission line, the FGF antenna should be added with a matching line. However, the height of the substrate is very small, thus the single matching line calculated is too narrow to realize. It is difficult to clip practically, so we can add a segment matching line using single nodal method so as to increase the width of the single matching line. The dimensions of the two matching lines are 16.7 mm × 2 mm and 65.2 mm × 13 mm respectively which are obtained by Advanced Design System (ADS), Agilent. This design is modeled and optimized using Computer Simulation Technology (CST). After that, the FGF antenna is characterized experimentally and compared to the copper antenna. As shown in Fig. 2d, the reflection coefficients of both antennas are around −12 dB while the resonant frequencies differ by 100 MHz. This discrepancy is derived from the different conductivities of the two materials. In addition, as shown in Fig. 2b and c, the far-field performances for the FGF and copper antennas are tested in a microwave anechoic
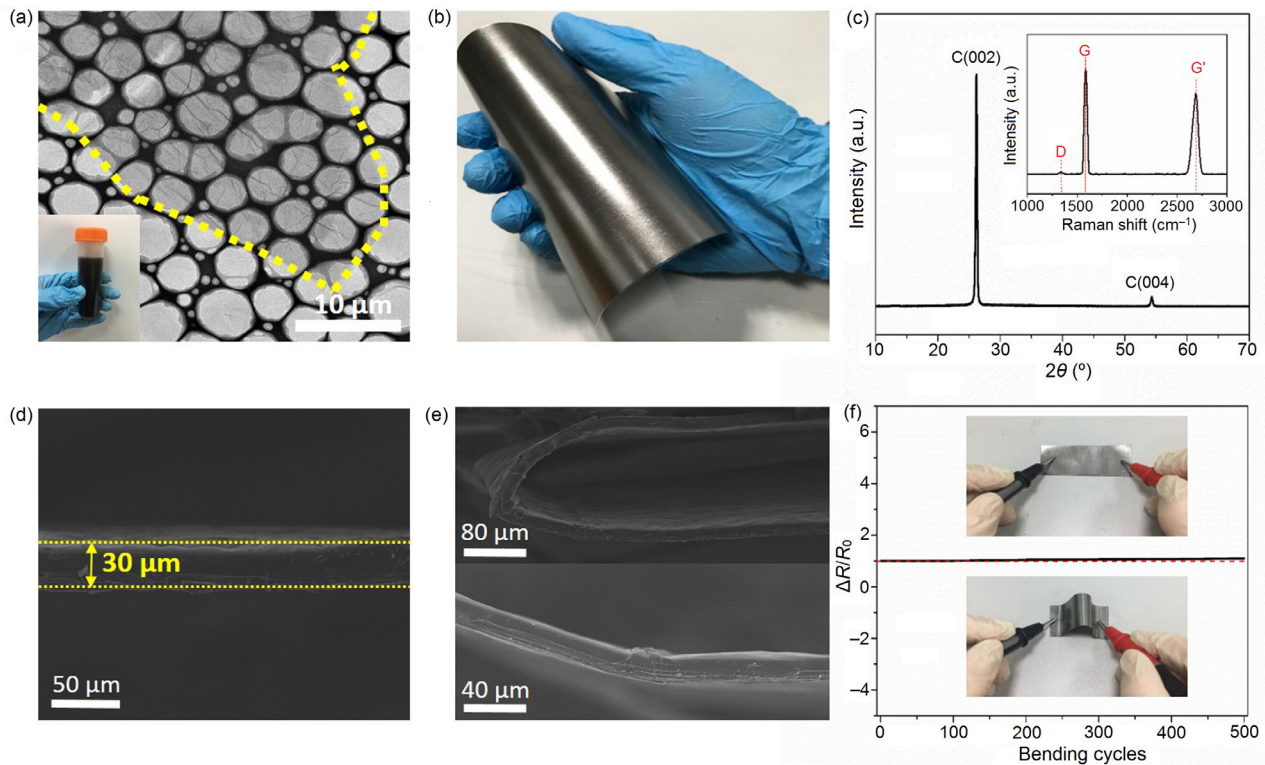
Fig. 1. (Color online) Sample preparation and characterization of the FGF. (a) TEM image of GO, inset is digital image of GO suspension. (b) Digital photograph of FGF under bending. (c) XRD patterns of FGF, inset is Raman spectra of FGF. (d) SEM image showing the cross-section of FGF with 30 μm thickness. (e) SEM images exhibiting FGF with 180° folding (up) and 150° bending (down). (f) Relative volume resistance of FGF with bending test. The bending state angle is approximately 70°.
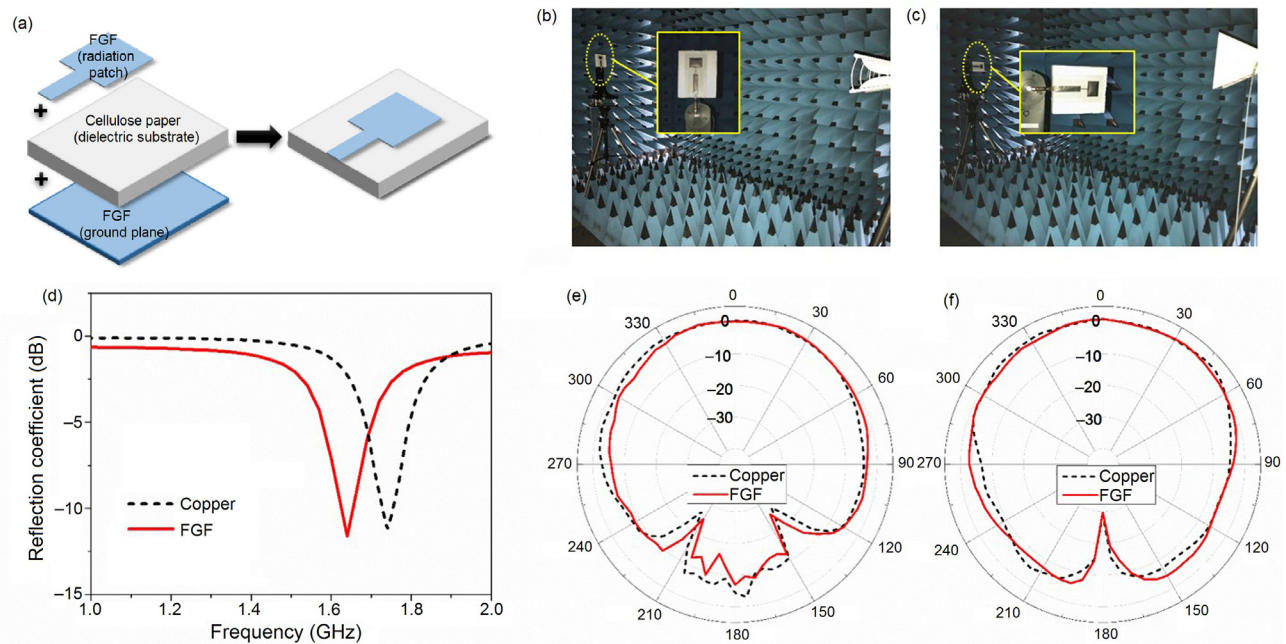

Fig. 2. (Color online) FGF antenna fabrication and performance measurement. (a) Schematic diagram of FGF antenna with paper substrate. (b) Photo of elevation plane measurement. (c) Photo of Azimuth plane measurement. (d) Measured reflection coefficients for FGF and copper antennas in the same condition. Comparison of measured normalized radiation pattern in the E-plane (e) and H-plane (f) for FGF and copper antennas at their respective resonant frequency.

chamber. Fig. 3e and f demonstrates the radiation patterns of FGF and copper antennas in the E-plane and the H-plane at their respective resonant frequency. It can be concluded from the plots that FGF antenna and copper antenna perform the same radiation pattern.

This FGF antenna can be seen as a bending strain sensor as shown in Fig. 3a. The sensor is subjected to compressive stress when it bends towards radiating patch and it is subjected to tensile stress when it bends towards ground plane. In order to test the mechanical flexibility of this FGF antenna sensor, it is attached to
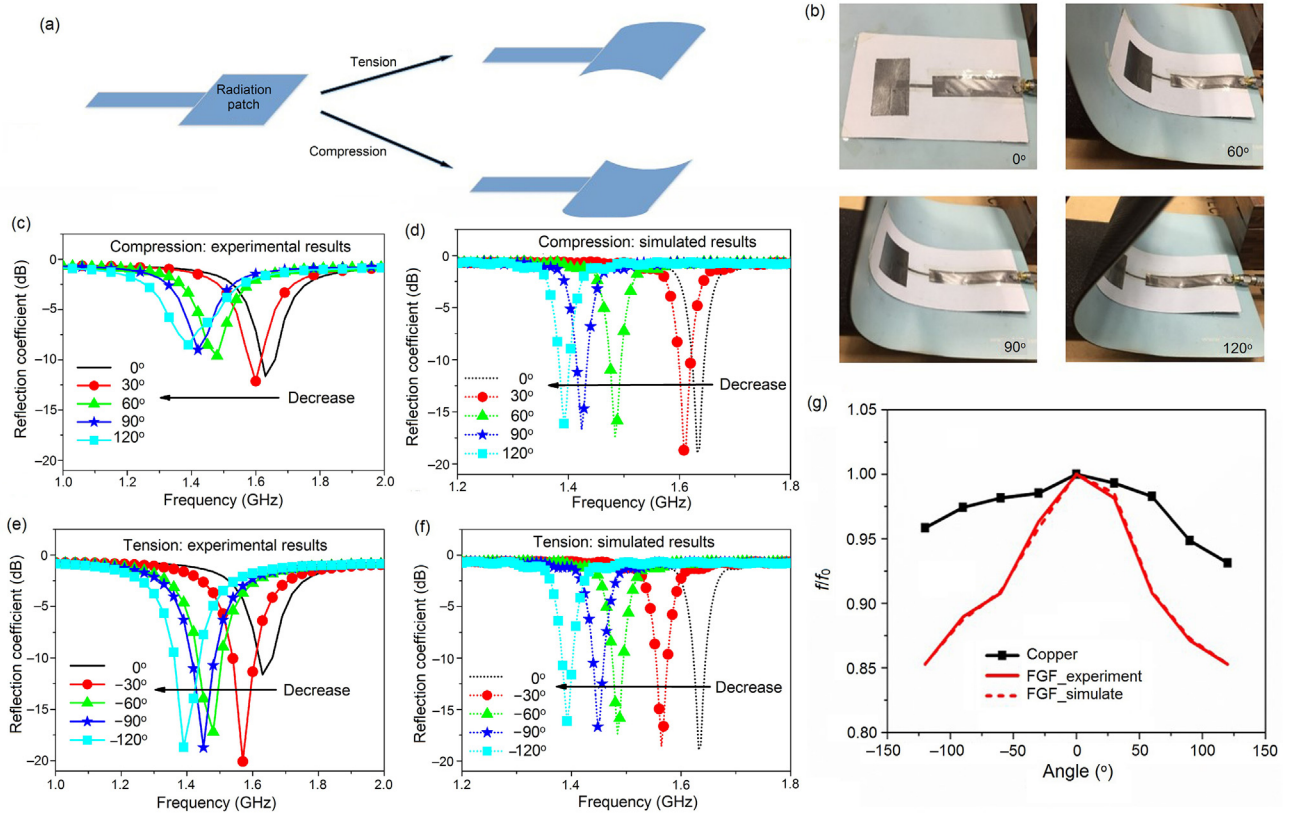
Fig. 3. (Color online) Tension and compression strain measurement based on the proposed antenna. (a) Schematic diagram of FGF antenna's tension and compression bending strain. (b) Photographs of a FGF antenna sensor attached to a soft mouse pad and bent at different angles. The reflection coefficient of experimental (c) and simulated (d) results under compression bending strain respectively. The reflection coefficient of experimental (e) and simulated (f) results under tension bending strain respectively. (g) Normalized resonant frequency of measured (thick solid line) and simulated (thick dash line) results compared with copper antenna (thin solid line) in the same condition.

a soft mouse pad and the resonant frequency of the antenna is measured by bending the mouse pad at different angles, as shown in Fig. 3b. The performance of the FGF antenna is measured using a Network Analyzer (Keysight N5225A) and the results are shown in Fig. 3c and e. Compared with the simulated results shown in Fig. 3d and f, the frequency responses of FGF antenna are generally consistent and the resonant frequency decreases with the increase of the bending angle no matter under compression bending strain or tension bending strain. One can observe that the compressive and tension strain cannot be distinguished from the resonant frequency shift data. However, the magnitudes at resonant frequencies of the measured reflection coefficient curves show the difference between the two cases. Generally, the magnitudes of measured reflection coefficient curves obtained from compression case are smaller than that from tensile case due to there are coupling effects occurred when bending the radiation part of antenna to microstrip line and coaxial cable part. As to the tension case, there is no coupling effect because of the ground plane, which results in sharper resonance of the curves. It should be noted that the sub-miniature-A (SMA) connector and the cable are not considered in simulation and that is the reason why there is no obvious difference between the simulated data of the two cases.

Eq. (5) shows that the bending radius r and the bending angle θ are in inverse proportion. L is physical length of FGF patch. Thus, the resonant frequency decreases with the drop of bending radius.

$$r = \frac{L}{\theta}. \tag{5}$$

Eq. (6) can be used to explain the reason.

$$f_{rq} = \frac{c}{2L_{eff}\sqrt{\varepsilon_{reff}}}, \tag{6}$$

where $L_{eff} = L + 2\Delta L$ and $L \gg \Delta L$.

The resonant frequency is associated with the antenna's effective length L_{eff} and the effective dielectric constant ε_{reff}. However, the physical length L is much greater than ΔL, the effective length L_{eff} can be seen as a constant. Hence, the alteration of resonant frequency is mainly related to the variation of effective dielectric constant ε_{reff}. The change of ε_{reff} can be explained by Eq. (7) [32].

$$\varepsilon_{reff} = \varepsilon_{r0}(1 + \eta h(d - 0.5)/r), \tag{7}$$

where ε_{reff} and ε_{r0} are the effective dielectric constants in bending state and relaxed state respectively, η denotes the proportionality factor, h is the height of the dielectric substrate, r indicates the bending radius, d represents a constant between 0.5 and 1. Under completely bending state, $d = 0.5$; for perfectly no bending state, $d = 1$.

Because ε_{reff} and r are in inverse proportion, ε_{reff} increases with the decrease of r. As a result, the resonant frequency and the bending radius are in direct proportion. What is more, ε_{reff} is related to the substrate's height h, which is independent of the operation frequency, so this principle can be applied to all frequencies. In consequence, the sensing principle of the FGF antenna sensor is based on the variation of effective dielectric constant when the antenna bends. And the effective dielectric constant will return to its original value when the paper patch antenna is in relaxed state.

In Fig. 3g, the positive portion and the negative portion of the plot represent this antenna bending towards radiator and ground plane respectively. It is observed that the normalized resonant frequency would decrease when bending the antenna to both directions with an increasing angle. Compared with the copper antenna with the same size, FGF antenna is obviously more

sensitive observed from Fig. 3g. And the sensitivity is a key feather to evaluate the flexibility of a sensor. It is proposed the normalized resonant frequency is f/f_0 and its variation $\Delta f/f_0 = (f - f_0)/f_0$, where f is the resonant frequency in bending state, f_0 is the resonant frequency in relaxed state. The sensitivity S is measured using the following relations [33]:

$$S = (\Delta f/f_0)/\Delta \xi, \tag{8}$$

$$\xi = (\pm)h/2r. \tag{9}$$

ξ is the bending strain of the sensor, r is the bending radius, and h is the thickness of the cellulose paper. The calculated sensitivity of this FGF antenna is around 9.8 for compressive bending and 9.36 for tensile bending, which is higher than that of copper antenna (5.39 for compressive bending and 4.05 for tensile bending) in GHz frequency range.

The reason for the significant differences in the antenna sensitivity is the differences of micro structure of the FGF and the copper. The FGF is a multi-layer structure, which is composed by tens of thousands of graphene nano flakes. There are two basic bonds of the FGF: one is the in-plane σ-bonds of the graphene nano flakes, which will provide a strong covalent connection between the atoms in horizontal plane [34]. Another one is the bond between the graphene layers, which is generally provided by external processing like high temperature and high pressure. Obviously, the bonds between layers are not that strong as the in-plane σ-bonds between the neighbor atoms. That is to say, when a strain is imposed on the FGF material, the bonds between the layers are easily affected, which will lead to a change of Ω contact. As a consequence, a large change of conductivity will happen and impedance matching will be adjusted. However, copper is a monocrystal material. The atoms of the copper film are all connected by the chemical bonding, which brings strong connection of both horizontal and vertical directions. When imposing an external force, the copper is not that affected like FGF on the conductivity and surface impedance. This would result in an antenna with a lower sensitivity than FGF antenna sensors.

Moreover, during the experiment, the frequency response of the device is abnormal when the bending angle is in the range of ±150°–±180°. In this range, two halves of FGF patches are close to each other in 180° phase shift, which would increase destructive interference and alter the radiation characteristics of the antenna, and thus the antenna becomes inoperable. These results indicate that the antenna based bending strain sensors can be utilized in robotic arm applications and in intelligent wireless monitoring of movements.

Besides, the mechanical flexibility and structure stability of the FGF antenna are significantly improved compared with the traditional metal antenna, which can extend the service life of the antenna. As shown in Fig. S2 (online), after several times deformation, the FGF antenna still looks flat and smooth, while the copper antenna shows obvious wrinkles.

Significantly, this FGF antenna sensor can be attached to human skin in the future for human motion detection. Different from some other sensors, this antenna sensor does not need communication equipment such as Bluetooth, ZigBee or WiFi for teletransmission information devices [35].

To show the versatility of the FGF material, two different substrates are used for loading the FGF antenna. Also, for maintaining the consistency, it only considers compression case in the test, and the test is shown as two different scenarios. In Fig. 4a and b, the FGF antenna on paper substrate is attached to the back of the hand with antenna part facing the human skin. When the hand clenched, the FGF antenna would show the compression case. Similarly, in Fig. 4c and d, the FGF antenna on PET substrate is adhered to human elbow with the ground plane touching the skin. When bending the elbow, the FGF antenna would display the compression motion as well. That is to say, two kinds of the motion are used in the test, but they are both compression test in fact. The measured data is shown in Fig. 4e. What we can get from this plot is that the FGF antenna is able to be paved on different substrate, and the resonant frequency shift varies with different substrates. What's more, the resonant frequency shift of antenna on paper substrate is larger than the one of antenna on PET substrate since the FGF can be closely attached to the paper substrate instead of PET substrate. After the deformed antenna returned to its original state, it maintains almost the same spectral properties with a resonant frequency shift less than 0.1% before and after deformation in each case.

For practical applications, the temperature and humidity are the two vital factors. Due to the limitation of the current equipment, only the effect of temperature is evaluated in this paper with a constant humidity. We record the experiment as shown in Fig. S3 (online). The result shows that there is no significant change of the working frequency (1.63 GHz), which suggests a stable FGF antenna sensor under environment with different temperatures. This is caused by the high thermal conductivity of 1,932.73 W/(m K) obtained in our previous work [36].
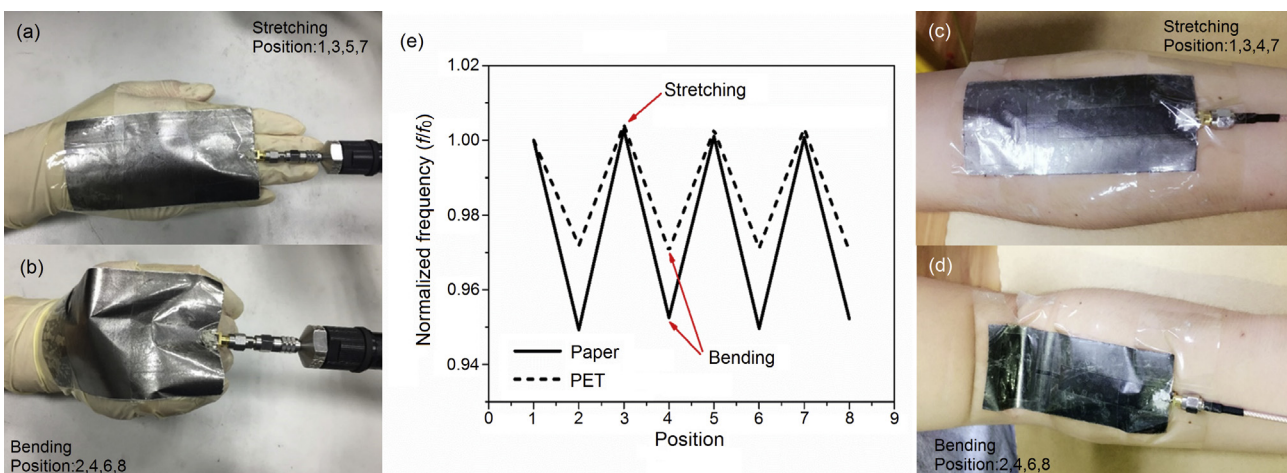

Fig. 4. (Color online) Photographs of a FGF antenna sensor attached to (a, b) the back of the hand joint based on paper and (c, d) the inside of the elbow based on PET. (e) Normalized frequency changing with stretching state and bending state.

4. Conclusions

In conclusion, this work for the first time demonstrates a wearable sensor based on a FGF antenna with high sensitivity, mechanical flexibility, reversible deformability and structure stability. Radiating properties of the FGF antenna are characterized under compressive and tensile strain, which is agreed well with the simulation results. Compared with the antenna sensor based on copper, this FGF antenna sensor shows much higher sensitivity and stability. In particular, when the FGF antenna sensor is under compressive bending and tensile bending, the measured sensitivity is up to 9.8 and 9.36 respectively, which is much higher than that of copper antenna sensor (5.39 for compressive bending and 4.05 for tensile bending). Moreover, this simple FGF film antenna sensor is further attached to human skin for simulating the actual wearable devices, and the test results show that the sensor can detect the bending of the joint well.

Conflict of interest

The authors declare that they have no conflict of interest.

Acknowledgments

Appendix A. Supplementary data

Supplementary data associated with this article can be found, in the online version, at https://doi.org/10.1016/j.scib.2018.03.014.

References

[1] Liao X, Liao Q, Yan X, et al. Flexible and highly sensitive strain sensors fabricated by pencil drawn for wearable monitor. Adv Funct Mater 2015;25:2395–401.
[2] White MS, Kaltenbrunner M, Głowacki ED, et al. Ultrathin, highly flexible and stretchable PLEDs. Nat Photon 2013;7:811–6.
[3] Wang C, Hwang D, Yu Z, et al. User-interactive electronic skin for instantaneous pressure visualization. Nat Mater 2013;12:899–904.
[4] Liu J, Yang C, Wu H, et al. Future paper based printed circuit boards for green electronics: fabrication and life cycle assessment. Energy Environ Sci 2014;7:3674–82.
[5] Lim B, Torati SR, Kim KW, et al. Concentric manipulation and monitoring of protein-loaded superparamagnetic cargo using magnetophoretic spider web. NPG Asia Mater 2017;9:e369.
[6] Liao Q, Mohr M, Zhang X, et al. Carbon fiber-ZnO nanowire hybrid structures for flexible and adaptable strain sensors. Nanoscale 2013;5:12350–5.
[7] Liao Q, Zhang Z, Zhang X, et al. Flexible piezoelectric nanogenerators based on a fiber/ZnO nanowires/paper hybrid structure for energy harvesting. Nano Res 2014;7:917–28.
[8] Chun J, Kang NR, Kim JY, et al. Highly anisotropic power generation in piezoelectric hemispheres composed stretchable composite film for self-powered motion sensor. Nano Energy 2015;11:1–10.
[9] Huo CX, Yan Z, Song XF, et al. 2D materials via liquid exfoliation: a review on fabrication and applications. Sci Bull 2015;60:1994–2008.
[10] Hempel M, Nezich D, Kong J, et al. A novel class of strain gauges based on layered percolative films of 2D materials. Nano Lett 2012;12:5714–8.
[11] Amjadi M, Pichitpajongkit A, Lee S, et al. Highly stretchable and sensitive strain sensor based on silver-elastomer nanocomposite. ACS Nano 2014;8:5154–63.
[12] Barlian AA, Park W, Mallon JR, et al. Review semiconductor piezoresistance for microsystems. Proc IEEE Inst Electr Electron Eng 2009;97:513.
[13] Xue P, Yang X, Lai X, et al. Controlling synthesis and gas-sensing properties of ordered mesoporous In_2O_3-reduced graphene oxide (rGO) nanocomposite. Sci Bull 2015;60:1348–54.
[14] Yan C, Wang J, Kang W, et al. Highly stretchable piezoresistive graphene-nanocellulose nanopaper for strain sensors. Adv Mater 2014;26:2022–7.
[15] Yamada T, Hayamizu Y, Yamamoto Y, et al. A stretchable carbon nanotube strain sensor for human-motion detection. Nat Nanotechnol 2011;6:296–301.
[16] Herrmann J, Müller KH, Reda T, et al. Nanoparticle films as sensitive strain gauges. Appl Phys Lett 2007;91:18–289.
[17] Zhang X, Chen Y, Ding SN. Facile and large-scale synthesis of green-emitting carbon nanodots from aspartame and the applications for ferric ions sensing and cell imaging. Sci Bull 2017;62:1256–66.
[18] Xiao X, Yuan L, Zhong J, et al. High-strain sensors based on ZnO nanowire/polystyrene hybridized flexible films. Adv Mater 2011;23:5440–4.
[19] Zhao J, Zhang GY, Shi DX. Review of graphene-based strain sensors. Chin Phys B 2013;22:35–43.
[20] Song RG, Wang QL, Mao BY, et al. Flexible graphite films with high conductivity for radio-frequency antennas. Carbon 2018;130:164–9.
[21] Wallace PR. The band theory of graphite. Phys Rev 1947;71:622–34.
[22] Slonczewski JC, Weiss PR. Band structure of graphite. Phys Rev 2008;21:2228–39.
[23] Sun C, Wen B, Bai B. Recent advances in nanoporous graphene membrane for gas separation and water purification. Sci Bull 2015;60:1807–23.
[24] Wang X, Hao J. Recent advances in ionic liquid-based electrochemical biosensors. Sci Bull 2016;61:1281–95.
[25] Shen B, Zhai W, Zheng W. Ultrathin flexible graphene film: an excellent thermal conducting material with efficient EMI shielding. Adv Funct Mater 2014;24:4542–8.
[26] Murakami M, Nishiki N, Nakamura K, et al. High-quality and highly oriented graphite block from polycondensation polymer films. Carbon 1992;30:255–62.
[27] Huang W, Drzal LT. Graphene nanoplatelet paper as a light-weight composite with excellent electrical and thermal conductivity and good gas barrier properties. Carbon 2012;50:1135–45.
[28] Xin G, Sun H, Hu T, et al. Large-area freestanding graphene paper for superior thermal management. Adv Mater 2014;26:4521–6.
[29] Teng C, Xie D, Wang J, et al. Ultrahigh conductive graphene paper based on ball-milling exfoliated graphene. Adv Funct Mater 2017;27:1700240.
[30] Peng L, Xu Z, Liu Z, et al. Ultrahigh thermal conductive yet superflexible graphene films. Adv Mater 2017;29:1700589.
[31] Wiley AJ. Antenna Theory Analysis and Design. 3rd ed. New Jersey: John Wiley & Sons; 2005.
[32] Boeykens F, Rogier H, Vallozzi L. An efficient technique based on polynomial chaos to model the uncertainty in the resonance frequency of textile antennas due to bending. IEEE Trans Antennas Propag 2014;62:1253–60.
[33] Kanaparthi S, Sekhar VR, Badhulika S. Flexible, eco-friendly and highly sensitive paper antenna based electromechanical sensor for wireless human motion detection and structural health monitoring. Extrem Mech Lett 2016;9:324–30.
[34] Geim AK, Novoselov KS. Flexible, the rise of graphene. Nat Mater 2007;6:183–91.
[35] Kanaparthi S, Badhulika S. Solvent-free fabrication of a biodegradable all-carbon paper based field effect transistor for human motion detection through strain sensing. Green Chem 2016;18:3640–6.
[36] Wang Z, Mao BY, Wang QL, et al. Ultrahigh conductive copper/large flake size graphene heterostructure thin-film with remarkable electromagnetic interference shielding effectiveness. Small 2018. https://doi.org/10.1002/smll.201704332.

Danli Tang was born in Hubei, China. She received the Bachelor of Science degree in electronic information science and technology from the Wuhan University of Technology, Wuhan, China, in 2015. Currently, she is pursuing the Master of Science degree in physics at the Hubei Engineering Research Center of RF-Microwave Technology and Application, School of Science, Wuhan University of Technology, Wuhan, China. Her research interests include conductive graphene films, electromagnetic device design and modelling.

Daping He is a full professor in Wuhan University of Technology, as a member of Hubei Engineering Research Center of RF-Microwave Technology and Application. His research interest is preparation and application of nano composite materials, such as the synthesis and structure control of advanced graphene materials, interface design of noble metal and application of these materials into new energy devices, sensors and RF microwaves field. He was awarded as Newton International Fellow in 2014 by the British Royal Society.